Applications of conjugated polymer based composites in wastewater purification

Yongshun Huang,[ab] Jiaxing Li,*[ac] Xiaoping Chen[d] and Xiangke Wang[ae]

The increasing water demand and the worldwide shortage of clean water call for new technologies for wastewater treatment, of which adsorption is a simple and efficient method to remove organic and inorganic pollutants from contaminated water. Conjugated polymers, particularly for polyaniline, polypyrrole, polythiophene and their derivatives/analogues, have been widely applied in wastewater purification due to their unique properties, such as easy synthesis, porous structure, tunable morphology, good electrorheological property, unique redox chemistry, non-toxicity, *etc.* This review summarizes potential solutions to wastewater treatment by utilizing conjugated polymer composites as adsorbents. The adsorption phenomenon is briefly introduced, followed by its mechanism investigation techniques. Detailed discussions are focused on the adsorption advantages of polyaniline, polypyrrole and polythiophene based composites to conventional materials. The remaining challenges are also mentioned.

1. Introduction

Water is of vital importance to human beings. However, as reported by the Encyclopedia Britannica, the directly accessible fresh water to human beings only occupies about 0.007% of all water on the Earth, which makes clean water scarcity a worldwide issue. Currently, 2.0 billion people lack clean drinking water, which may reach 4.6 billion in 2080, according to the World Bank report.[1] The generation of a huge amount of hazardous chemical waste from various industries (*e.g.* effluents from paper, textile, fertilizer or petrochemical industries, electroplating plants, tanneries and slaughterhouses) and its improper disposal further exacerbates the water crisis. The statistical data from the UN water organization indicate that in most of the developing countries, about 90% of the polluted water is directly discharged into rivers, lakes or coastal shores without any purification treatment.[2] These contaminants include conventional pollutants (*e.g.* heavy metal ions and distillates), micro-pollutants (*e.g.* microcystins and antibiotics) and dyes (*e.g.* methylene blue, methyl orange, rhodamine B, *etc.*). Those contaminants are major threat for human health,

[a]*School of Environment and Chemical Engineering, North China Electric Power University, Beijing, 102206, P. R. China. E-mail: lijx@ipp.ac.cn; Fax: +86-551-65591310; Tel: +86-551-65592788*

[b]*Department of Chemistry, The University of Cincinnati, Cincinnati, OH, 45221, USA*

[c]*Institute of Plasma Physics, Chinese Academy of Sciences, P.O. Box 1126, Hefei, 230031, P. R. China*

[d]*CirQuest Labs LLC and Ariste Medical, Memphis, TN, 38103, USA*

[e]*Faculty of Engineering, King Abdulaziz University, Jeddah, 21589, Saudi Arabia*

Yongshun Huang received his Bachelor degree in Chemistry from Yangzhou University in 2005. He obtained two Master degrees from University of Science and Technology of China and University of Colorado at Boulder. Then, he worked in a pharmaceutical company on DNA/RNA oligomer synthesis and modification. Currently, he is pursuing his PhD at The University of Cincinnati, focusing on the design and synthesis of blood compatible biomaterials.

Jiaxing Li studied chemistry in Lanzhou University and received BS in 2001. He completed PhD in Organic Chemistry from University of Science and Technology of China in 2008. After graduation, he joined Institute of Plasma Physics, Chinese Academy of Sciences. Currently, he mainly focuses on the physicochemical behavior of heavy metal ions and radionuclides in the environment, and the application of nanomaterials in pollution management. He published more than 60 papers and 3 patents.

food security and access to safe drinking water. All of these problems call for the suitable water purification techniques, employing various mechanical, biological and chemical purification methods. Biological methods use bacteria to decompose the pollutants or to oxidize/reduce toxic chemicals into non-toxic compounds whereas mechanical methods utilize settling techniques to accumulate and separate the pollutants. In contrast, the chemical methods involve ion exchange, chemical oxidation/reduction and chemical adsorption techniques. The ion exchange is performed to soften the water by exchanging the hard magnesium or calcium cations with soft sodium cations. Similarly, during the chemical oxidation/reduction process, pollutants undergo structural modifications and transform into less toxic or even non-toxic compounds. In the past, conjugated polymers, particularly those based on polyaniline (PANI), polypyrrole (PPy), polythiophene (PT) and their derivatives/analogues, have gained popularity as chemical adsorbents due to their ease of synthesis, porous structure, tunable morphology, good electrorheological property, unique redox chemistry, non-toxicity, insolubility in water and reversible ion (especially cation) sorption/desorption capability.[3–10] However, despite much progress, challenging issues still exist, such as their low adsorption capacity, poor recyclability, high cost and difficulties in porosity control, to name a few. Recently, efforts have been devoted to combine the conjugated polymers with conventional organic/inorganic adsorbents (*e.g.* activated charcoal, carbon black, carbon nanotubes, graphene/graphene oxide, sawdust, husks, silicates, clays, zeolites and so on) to form composite adsorbents.[11–21] These composites combine specific advantages of both partners and display enhanced purification response to the involved physical/chemical adsorption as well as adsorption processes. Despite the extensive reviews on the properties and applications on PANI,[22–30] PPy[30–33] and PT,[34–38] the applications in wastewater treatment have not been reviewed. In this review, the conjugated polymer based composites will be discussed for their applications in adsorptive purification of polluted water.

2. Adsorption phenomenon

Adsorption is a binding process of a gas or liquid solute to accumulate on the surface of a solid or a liquid (adsorbent) with the formation of a molecular or atomic film (the adsorbate). Different from adsorption, absorption requires a substance to permeate or dissolve into a liquid or solid. A combination of adsorption and absorption is called sorption and the reverse of adsorption is called desorption. A schematic representation is depicted in Fig. 1.

The widely application of adsorption technique involves the physical, chemical and biological systems, as well as the industrial applications. Depending on the adsorbed nature of binding, the adsorption process can be classified as physisorption and chemisorption. Physisorption binds adsorbates *via* non-covalent interactions, while chemisorption forms covalent bonds between the adsorbates and adsorbents. Most of the conjugated polymer composites take advantage of physisorption by either ionic exchange of doping/reversible redox

Fig. 1 Schematic illustration of absorption (a) and adsorption (b) phenomenon.

Xiaoping Chen received his PhD in polymer chemistry from The University of Cincinnati in 2013. His PhD research focused on the polyurea peptoid synthesis with further modification by RAFT polymerization. Currently, he is working in Ariste Medical as a polymer chemist, focusing on the development of implantable medical devices (hernia mesh, vascular grafts, and stents), containing therapeutic reagents.

Xiangke Wang is a professor of Institute of Plasma Physics, Chinese Academy of Sciences. He received his BS in 1995 and his PhD in 2000 from Lanzhou University. Then, he joined SUBATECH Laboratory (France) as a research fellow and Karlsruhe Research Center (Germany) as Alexander von Humboldt research fellow. He focuses on the application of plasma technique in the synthesis of nanomaterials and their applications in energy and environmental pollution management, and also radionuclide physicochemical behavior in the environment. He has published over 140 papers in peer-review journals.

reaction or molecular interactions, such as van der Waals forces, hydrophobic effects, π–π interaction, hydrogen-bonding, electrostatic interactions, *etc.* The driving force of adsorption is the reduction of interfacial tensions between the adsorbates and adsorbents, which can be influenced by the surface area, pore size/size distribution, surface affinity/wettability and so on. The efficiency of adsorption is often described by isotherms, kinetics and thermodynamics.

2.1 Adsorption isotherms

To understand the adsorption mechanism, an adsorption isotherm is often applied to describe the adsorbed adsorbates *versus* the equilibrium concentration, which illustrates the efficiency of the adsorption, how the adsorption system proceeds, *etc.* Several adsorption isotherms have been proposed, and the experimental data are often used to follow these isotherms to investigate the adsorption mechanisms.

2.1.1 Langmuir adsorption isotherm. The Langmuir theory describes the quantitatively formation a monolayer adsorbate on the outer surface of the adsorbent without further adsorption.[39,40] This model assumes an adsorption homogeneity, which includes the equally available adsorption sites, monolayer surface coverage and no mutual interactions. The equation of Langmuir adsorption isotherm is expressed in eqn (1).

$$q_e = \frac{K_L q_m C_e}{1 + K_L C_e} \tag{1}$$

After transformation, eqn (1) can be converted into a linear eqn (2):

$$\frac{C_e}{q_e} = \frac{1}{K_L q_m} + \frac{C_e}{q_m} \tag{2}$$

where C_e is the equilibrium concentration of the adsorbate remained in solution (mg L^{-1}), q_e is the adsorbed amount (mg g^{-1}), q_m (mg g^{-1}) is the maximum adsorption capacity, which stands for the amount of the adsorbate at complete monolayer coverage, and K_L (L mg^{-1}) is a Langmuir constant that relates to the adsorption rate. The essential features of the Langmuir isotherm can be expressed as R_L, a dimensionless constant used to express as separation factor or equilibrium parameter (eqn (3)).[41]

$$R_L = \frac{1}{1 + K_L C_0} \tag{3}$$

where C_0 is the initial concentration of the adsorbate (mg L^{-1}), R_L is the Langmuir constant related to the energy of adsorption, which can be unfavorable ($R_L > 0$), linear ($R_L = 1$), favorable ($0 < R_L < 1$) or irreversible ($R_L = 0$).

2.1.2 Freundlich adsorption isotherm. The Freundlich isotherm model is usually applied to the heterogeneous surfaces. It is an empirical relationship, implying the binding energies of the adsorbate related to the adjacent sites. This model has the following form, eqn (4).[42–44]

$$q_e = K_F C_e{}^n \tag{4}$$

A linear form can also be expressed in eqn (5), as shown below.

$$\log q_e = \log K_F + n \log C_e \tag{5}$$

K_F (mg^{1-n} L^n g^{-1}) and n are the Freundlich constants, representing the adsorption capacity when the adsorbate equilibrium concentration equals to 1, and the adsorption intensity, respectively.

2.1.3 Dubinin–Radushkevich adsorption isotherm. Dubinin–Radushkevich (D–R) isotherm model is more applicable than the Freundlich isotherm since it is not limited by the heterogeneous surface and constant adsorption potential assumption. The D–R equation has the general expression as eqn (6):[45]

$$q_e = q_m \exp(-\beta \varepsilon^2) \tag{6}$$

The expression in a linear form is shown as eqn (7):

$$\ln q_e = \ln q_m - \beta \varepsilon^2 \tag{7}$$

where q_e and q_m are defined as above, β represents the activity coefficient related to the average adsorption energy (mg^2 kJ^{-2}), and ε is the Polanyi potential, which can be calculated from eqn (8):

$$\varepsilon = RT \ln\left(1 + \frac{1}{C_e}\right) \tag{8}$$

It should be mentioned that the D–R isotherm model is temperature-dependent, which means that when plotted $\ln q_e$ *versus* ε^2 at different temperatures, all suitable data will lie on the same curve, called characteristic curve.

2.1.4 Tempkin adsorption isotherm. The Tempkin isotherm describes the adsorbent–adsorbate interactions, which assumes that the adsorption heat decreases linearly rather than logarithmic as the coverage proceeds.[46] Besides, the derivation of this adsorption is characterized by a uniform distribution of binding energy, which can up to some maximum binding energy. The equation for this model is expressed as eqn (9):

$$q_e = \frac{RT}{b} \ln(k_t C_e) \tag{9}$$

A linear expression can be obtained as eqn (10):

$$q_e = B \ln k_t + B \ln C_e \tag{10}$$

where $B = \frac{RT}{b}$, k_t and B can be calculated by plotting q_e *versus* $\ln C_e$. k_t is the Tempkin constant and B is related with the heat of the adsorption.

Among various isotherms, Langmuir and Freundlich are found to be the two most popular models. It is important to point out that the above isotherms are often applied to the adsorptions case by case. One model may be suitable for particular "adsorbent–adsorbate–dispersion medium" system

whereas deviates for other systems. However, by plotting the suitable terms to obtain linear lines, the regression constants can be obtained such that the higher regression constant for particular model indicates its more suitability towards the concerned system.

Fox example, Fig. 2 showed the linear plots of PANI, its sawdust and rice husk based composites for Cr(III) removal under Langmuir and Freundlich adsorption regimes.[47] The corresponding linear regression parameters (Table 1) revealed that the Freundlich isotherm model fitted better than Langmuir when isolated PANI was used as an adsorbent, which can be ascribed to the multilayer physisorption of Cr(III) on PANI. In contrast, Langmuir isotherm model fitted better for PANI/sawdust and PANI/rice husk composites, indicating the homogeneous distribution of active sites on the composite surface, which resulted in chemisorption of Cr(III) on the adsorbent.

Compared with PANI/sawdust and PANI/rice husk composites, PANI/graphene oxide composites exhibited better linear regression parameters, as shown in Table 2.[48] Both PANI and PANI/graphene oxide followed Langmuir isotherm model with high regression coefficients of 0.995 and 0.998, respectively.

Other examples involve the adsorption isotherms of PPy/saw dust composites. It was observed that the adsorptions of carmoisine,[49] methylene blue,[50] and phosphate[51] fitted the Langmuir model, while Cr(VI)[52] and Zn(II)[53] adsorptions were suitable for Freundlich isotherms. The D–R isotherm model was also applied in some cases, such as the adsorption of fluoride[54] and Cr(VI)[55] by polypyrrolium chloride complex, which also followed the Freundlich isotherms.

2.2 Adsorption kinetics

As a fundamental method to monitor the adsorption efficiency, the adsorption kinetics are often used to predict the adsorption characteristics and mechanisms. The kinetic models involve pseudo-first order,[56] pseudo-second order,[57] Elovich[58,59] and intraparticle[60,61] diffusion model, of which the pseudo-first and
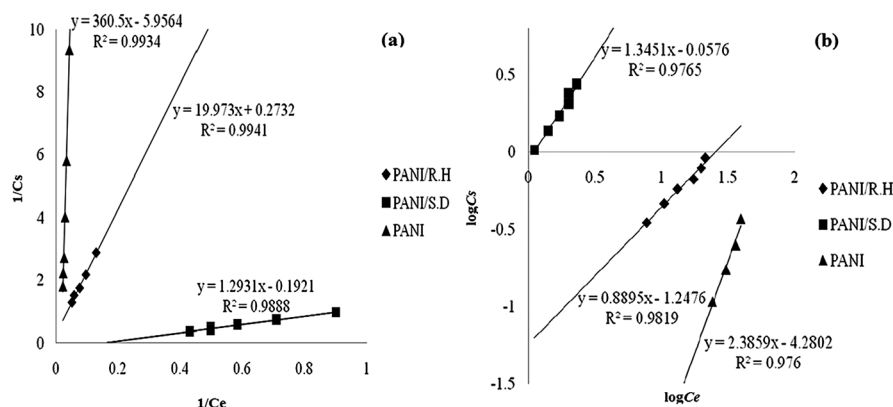

Fig. 2 Langmuir isotherm (a) and Freundlich isotherm (b) for Cr(III) adsorption by pure PANI, its rice husk and sawdust based composites. Reprinted from ref. 47 with permission from Sociedad Chilena de Química (2014).

Table 1 Isothermal and thermodynamic parameters for Cr(III) adsorption. Reprinted from ref. 47 with permission from Sociedad Chilena de Química (2014)

Adsorbent	Langmuir isotherm parameters			Freundlich isotherm parameters			Thermodynamic parameter
	R^2	q_m (mg g^{-1})	K_L (L mg^{-1})	R^2	K_F	n	$\Delta G^{\neq}$ (kJ mol^{-1})
PANI	0.988	0.165	16	0.989	0.0053	2.381	−10.245
PANI/rich husk	0.990	4.739	10	0.982	0.057	0.888	−11.410
PANI/sawdust	0.988	5.128	150	0.976	0.877	1.345	−4.700

Table 2 Isothermal parameters for Cr(VI) adsorption. Reprinted from ref. 48 with permission from The Royal Society of Chemistry (2013)

Adsorbent	Langmuir isotherm parameters			Freundlich isotherm parameters		
	q_m (mg g^{-1})	K_L (mg^{-1})	R^2	K_F	n	R^2
PANI	490.2	0.19	0.995	79.25	2.04	0.937
PANI/graphene oxide	1149.4	0.042	0.998	123.59	2.22	0.976

pseudo-second order equations are listed as eqn (11) and (12), respectively.

$$\ln(q_e - q_t) = \ln q_e - k_1 t \qquad (11)$$

$$\frac{t}{q_t} = \frac{1}{k_2 q_e^2} + \frac{t}{q_e} \qquad (12)$$

where q_e and q_t (mg g^{-1}) are the amount of adsorbates at equilibrium and at time t, respectively, while k_1 (h^{-1}) and k_2 (g mg^{-1} h^{-1}) are the rate constants for pseudo-first and pseudo-second order models.

The equations for the Elovich[58,59] and intraparticle[60,61] model can be written as eqn (13) and (14), respectively.

$$q_t = \frac{\ln(\alpha\beta)}{\beta} + \frac{\ln t}{\beta} \qquad (13)$$

$$q_t = k_{ip} t^{0.5} + C \qquad (14)$$

where α and β are the constants during the adsorption process, and k_{ip} (g mg^{-1} h$^{-0.5}$) is the intraparticle diffusion rate constant. A plot of q_t vs. $\ln t$ should give a linear relationship for its applicability with a slope of $(1/\beta)$ and an intercept of $(1/\beta)$ $\ln(\alpha\beta)$. The intraparticle diffusion model often involves two or more stages in the adsorption process, and any stage can be the rate-controlling stage.

Similar as the adsorption isotherms, the validity of the kinetic models can also be verified by plotting linear lines with a comparison of the regression constants. A higher linear regression constant indicates a more suitable model, and a faster equilibrium can be reached with a larger value of the rate constant. Currently, most adsorption processes fit well with pseudo-second order over the other models.

The adsorption of methylene blue by PANI/silica nanotube composite is a typical example, as depicted in Fig. 3 and Table 3.[62] The corresponding linear regression parameters indicated that pseudo-second order kinetic equation was more suitable than pseudo-first order and intraparticle diffusion kinetics.

Other examples involve the adsorptions of Cr(VI)[63] and Congo red[64] by PANI/PPy composite, Hg(II)[65] by PANI/humic acid composite and so on. Pseudo-first order model is also observed with an example of the competitive adsorption of reactive orange 16 and reactive brilliant blue R by PANI/bacterial extracellular polysaccharide composite.[66]

2.3 Adsorption thermodynamics

Thermodynamic investigations can also give useful information about the adsorption nature. The related constants, Gibbs free energy change (ΔG), enthalpy change (ΔH) and entropy change (ΔS), illustrate the thermodynamic feasibilities and the spontaneous nature of the process. By investigating the reaction at different temperatures, different equilibrium constants (k_d) can be obtained via the following eqn (15):

$$k_d = \frac{C_e}{C_{e,0}} \qquad (15)$$

where C_e and $C_{e,0}$ (mg L^{-1}) are the equilibrium concentration adsorbed on adsorbent and the equilibrium concentration of adsorbate in the solution, respectively. With different k_d at various temperatures, the Gibbs free energy change, enthalpy

Fig. 3 The pseudo-first order (a), pseudo-second order (b) and intraparticle diffusion kinetic plot for methylene blue adsorption by PANI/silica nanotube composite. Reprinted from ref. 62 with permission from Elsevier (2012).

Table 3 Kinetic parameters for methylene blue adsorption by PANI/silica nanotube composite. Reprinted from ref. 62 with permission from Elsevier (2012)

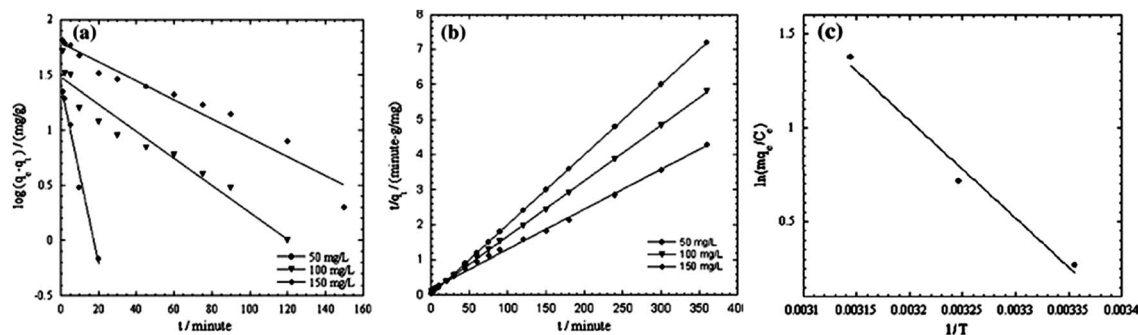| Models	Model parameters	R^2
Pseudo-first order	$q_e = 2.69$ mg g^{-1}, $k_1 = 0.69$ min^{-1}	$R^2 = 0.952$
Pseudo-second order	$q_e = 5.7$ mg g^{-1}, $k_2 = 0.09$ g mg^{-1} min^{-1}	$R^2 = 0.999$
Intraparticle diffusion	$k_{ip} = 0.9$ mg g^{-1} min^{-1}, $t^{0.5} = 3.55$ min, $C = 1.659$ mg g^{-1}	$R^2 = 0.977$

Fig. 4 Pseudo-first order (a) and pseudo-second order (b) kinetic models, as well as thermodynamic parameter plot, for Cr(VI) adsorption onto PPy/Fe$_3$O$_4$ nanocomposite. Reprinted from ref. 67 with permission from Elsevier (2011).

change and the entropy change can be obtained as from eqn (16) and (17).

$$\Delta G^0 = -RT \ln k_d \qquad (16)$$

$$\ln k_d = \frac{\Delta S^0}{R} - \frac{\Delta H^0}{RT} \qquad (17)$$

By plotting $\ln k_d$ *versus* $1/T$, the enthalpy and entropy change can be obtained, as well as the Gibbs free energy change. A negative value of Gibbs free energy and enthalpy indicates a spontaneous adsorption and an exothermic process. Most adsorption processes are spontaneous with minor exceptions.

The sorption of Cr(VI) by PPy/Fe$_3$O$_4$ nanocomposite is a typical example.[67] The pseudo-first order and pseudo-second order kinetic models were listed in Fig. 4, as well as the thermodynamic parameter plot, with the corresponding linear regression parameters in Table 4, which revealed that the pseudo-second order kinetic model gave better correlation than pseudo-first order kinetic model. The change in enthalpy and entropy were determined by the thermodynamic parameter plot of 43.4 kJ mol^{-1} and 147.73 J mol^{-1} K^{-1}, respectively. The Gibbs free energy changes, calculated from eqn (16), were -0.565, -2.04 and -3.51 kJ mol^{-1} at 298, 308 and 318 K, respectively, indicating a spontaneous and endothermic adsorption process.

Other negative Gibbs free energy changes involve the removal of Cr(VI)[67] and fluoride[68] by PPy/magnetic Fe$_3$O$_4$ and the Zn(II)[53] and nitrate[69] removal by PPy/saw dust with either positive or negative values of enthalpy or entropy. The exceptional positive Gibbs free energy was also observed for the adsorption of trichloroacetic acid by PPy/Th(IV) phosphate.[70]

3. PANI related composites in water purification

PANI is one of the earliest known synthetic polymers, which can date back to 1835 as "aniline black" for any products produced by the oxidation of aniline. The interest toward PANI increased significantly over the past decades due to its low cost, easy preparation, high conductivity, mechanical flexibility, environmentally stability and unusual doping/dedoping chemistry. Besides, PANI also has three distinct oxidation states with different colors, naming leucoemeraldine, emeraldine and pernigraniline.

The application of PANI as adsorbents for water purification is due to its large amount of amine and imine functional groups, which are expected to interact with inorganic ions and organic compounds, such as Hg(II),[71] Cr(VI),[72] methylene blue,[3,4] antibiotic drugs, and diclofenac sodium.[7] However, bare PANI particles can easily aggregate due to the inter- and intra-molecular interactions, which significantly reduce the surface area, resulting lower adsorption abilities. Other functional materials, including silica, sawdust, carbon nanotubes, graphene/graphene oxide, cellulose acetates, inorganic salts and organic molecules, are combined with PANI to generate PANI based composites to improve its surface area and to change its surface morphology. Depending on the nature of the incorporating functional materials, the PANI based composites can be discussed as PANI/inorganic material composites and PANI/organic material composites.

3.1 PANI/inorganic composites

The inorganic materials involve the silica, montmorillonite, attapulgite, Fe$_3$O$_4$, ZnCl$_2$, CuCl$_2$, *etc.* The as-prepared composites can adsorb various organic and inorganic pollutants from aqueous solutions.

Different silica crystalline forms were utilized to fabricate unique PANI/silica composites for wastewater purification. PANI were coated on silica gel to modify its surface morphology

Table 4 Kinetic parameters for Cr(VI) adsorption onto PPy/Fe$_3$O$_4$ nanocomposite. Reprinted from ref. 67 with permission from Elsevier (2011)

C_0 (mg L^{-1})	Pseudo-first-order model			Pseudo-second-order model		
	K_1 (min^{-1})	q_e (mg g^{-1})	R^2	K_2 (g mg^{-1} min^{-1})	q_e (mg g^{-1})	R^2
50	0.188	4.15	0.987	0.037	50.00	1.00
100	0.028	4.39	0.935	0.003	63.29	0.999
150	0.019	6.03	0.950	0.0007	87.71	0.996

and to improve its capacity for phenol[73] and acid green 25 (ref. 74) adsorption from aqueous solutions.

The SEM images of PANI and PANI/silica composite are illustrated in Fig. 5. PANI was 100 to 300 nm in diameter and 2 to 40 μM in length with visual noticeable cavities. However, the PANI/silica composite appeared as cluster spots with increased surface area, which in turn helped to increase the adsorption rate toward acid green 25.[74] The adsorption process was revealed to be pseudo-second order kinetic model and Langmuir isotherm, as shown in Fig. 5. The regression constants were 0.9894, 0.9995, 0.9961 and 0.9945 for pseudo-first, pseudo-second order kinetic models, the Langmuir and Freundlich isotherms, respectively.

Fig. 5   SEM images of PANI nanotube (a) and PANI/silica composite (b); pseudo-first (c), pseudo-second (d) order adsorption kinetics, and the Langmuir (e) and Freundlich (f) isotherms of PANI/silica composite to acid green 25 adsorption. Reprinted from ref. 74 with permission from Springer (2012).

Hexagonally ordered silica, SBA-15, were also fabricated with PANI to prepare PANI/hexagonally ordered silica nanocomposite, which was used to extract polycyclic aromatic hydrocarbons from aqueous solutions, including naphthalenes, biphenyl, acenaphthene, anthracene, and pyrene.[75] The same nanocomposite exhibited selective adsorption toward 2,4-dinitrophenol in aqueous solution in the presence of phenol with an adsorption capacity of 55.0 mg g^{-1}.[76] Chemical oxidation of aniline on hexagonal mesoporous silica (HMS) was carried out to generate PANI/HMS nanocomposite for Ni(II) elimination from aqueous solutions.[77] This process was spontaneous and endothermic, and can be applied to Freundlich isotherm and a pseudo-second order kinetic. The removal efficiency was 99.87% for 50 mg L^{-1} Ni(II) solution, and the maximum sorption capacity reached up to 253.17 mg g^{-1} at 300 mg L^{-1} Ni(II) solution. Desorption of Ni(II) from PANI/HMS nanocomposite was also investigated by using 0.1 M H$_2$SO$_4$ solution with a maximum desorption efficiency of 86%. After a three adsorption/desorption cycles, the removal efficiency was reduced less than 10%. 2,6-Dichlorophenol can also be selectively removed from aquatic environment by PANI/silica gel composite.[78] A spontaneous and endothermic process was also observed with a Langmuir isotherm.

Magnetic PANI/Fe$_3$O$_4$ nanocomposites were prepared *via* emulsion polymerization to remove nitrate ions,[79] which gave linear correlation to Freundlich isotherm with a pseudo-second order kinetic mechanism. The optimum sorption condition was found to be a 4.0 g L^{-1} sorbent solution with a contact time of 10 min at pH 7.0. PANI doped ZnCl$_2$ and CuCl$_2$ were used for sodium dodecyl benzene sulfonate (SDBS) removal in a spontaneous and exothermic process.[80] Toxic metallic cations, such as Cr(VI) and Hg(II), can also be adsorbed by the as-prepared composites. Flake-like PANI/montmorillonite nanocomposites for Cr(VI) removal were fabricated by *in situ* chemical oxidation.[81] A much lower desorption efficiency (12.3%) was observed, which was ascribed to the reduction of adsorbed Cr(VI) to Cr(III). Hg(II) removal by PANI/attapulgite composite was also observed.[82] The maximum adsorption capacity on Hg(II) was over 800 mg g^{-1}, which was predominantly controlled by chemical process and can be desorbed by a solution of 75% acetic acid and 1% thiocarbamide. The adsorption capacity is

maintained at 93% even after the fifth adsorption/desorption cycle.

Besides magnetic PANI/Fe$_3$O$_4$ nanocomposites, PANI/CoFe$_2$O$_4$ magnetic photocatalysts were also fabricated by *in situ* oxidative polymerization to remove various dyes, which included anionic dyes, methyl orange (MO), weak acid light yellow G (AY), weak acid black BR (AB), reactive black 39 (RB), and reactive yellow 145 (RY), neutral dye of neutral dark yellow GL (NY), and cationic dyes of methylene blue (MB) and Rhodamine B (RhB).[83] No obvious adsorption was observed for CoFe$_2$O$_4$ particles, while the PANI/CoFe$_2$O$_4$ magnetic photocatalysts exhibited significant adsorption capacities to the anionic and neutral dyes, which were attributed to the electrostatic interactions between the negative charged dyes and the positive charged PANI backbone. The electrostatic repulsion between cationic dyes and positive PANI resulted in poor adsorption, as observed in Fig. 6. Based on the correlation coefficient, this adsorption process belonged to the Langmuir isotherm and the pseudo second-order adsorption kinetics model (Table 5).

3.2 PANI/organic composites

Natural occurring sawdust, polysaccharides and carbon related materials have been fabricated with PANI and widely applied in wastewater purification.

PANI/sawdust composites have been applied to adsorb diclofenac sodium,[17] Cd(II),[12] Cu(II)[84] and Cr(VI).[85] The average

Table 5 Kinetic parameters for the adsorption of various dyes by PANI/CoFe$_2$O$_4$. Reprinted from ref. 83 with permission from The Royal Society of Chemistry (2012)

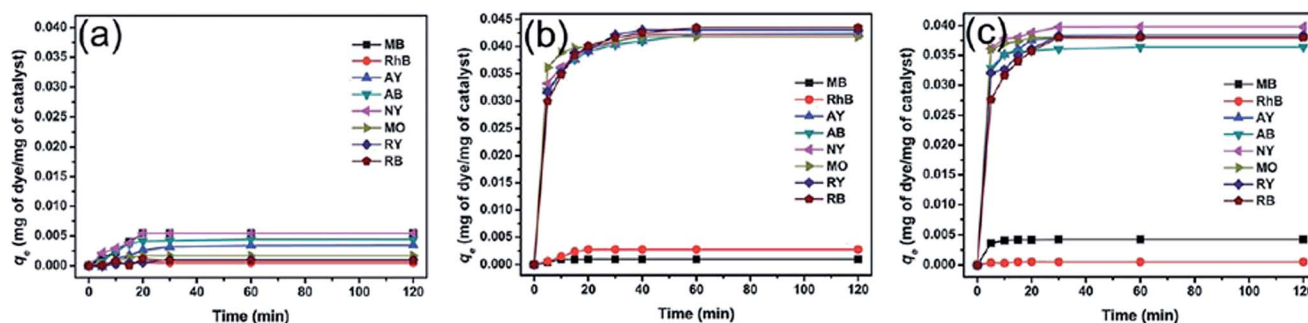| Dye	Langmuir isotherm		The second-order model		
	q_m	R^2	q_e	$k_s q_e^2$	R^2
MO	0.124	0.999	0.0418	0.0539	0.999
AB	0.120	0.998	0.0424	0.0238	0.999
AY	0.0915	0.999	0.0424	0.0238	0.999
NY	0.0804	0.999	0.0422	0.0282	0.999
RB	0.0726	0.999	0.0435	0.0177	0.998
RY	0.0779	0.999	0.0430	0.0219	0.999

Fig. 6 Adsorption capacity of various dyes with time in the presence of (a) CoFe$_2$O$_4$, (b) PANI/CoFe$_2$O$_4$, and (c) PANI. Reprinted from ref. 83 with permission from The Royal Society of Chemistry (2012).

adsorption capacity for Cu(ɪɪ) was report as high as 58.23 mg g^{-1},[84] while Cd(ɪɪ) was removed by pseudo-second order kinetics and a Freundlinch model.[12] Acidic condition (pH $\leq$ 2) was required for Cr(vɪ) removal and the mechanism was proposed *via* an anion exchange process.[85]

As for PANI/polysaccharide composite, PANI/extracellular composite had successfully applied for anionic reactive dyes removal, such as reactive brilliant blue R and reactive orange 16.[66] The electrostatic interactions between dye anions and cationic ammonium in the composite were ascribed to the adsorption process with the maximum adsorption capacities of 0.5775 mmol g^{-1} and 0.4748 mmol g^{-1} for reactive brilliant blue R and reactive orange 16, respectively. The effect of substituted aniline to the adsorption efficiency was investigated by synthesizing several poly(alkyl-substituted aniline)/chitosan composites.[86] Poly(*N*-ethylaniline)/chitosan composite exhibited the highest removal ability to Cr(vɪ) of 229.8 mg g^{-1}. This process was mainly controlled by physical adsorption. The fabrication of PANI/cellulose acetate composite for gold-iodide complex removal was comprehensively investigated.[87,88] The AuI_2^- was proposed to exchange with the Cl^- during the adsorption (Fig. 7). This process can adsorb 94% AuI_2^- with a solid/liquid ratio of membrane of 40 g L^{-1}. The advantageous adsorption ability of PANI–hydroxypropylcellulose/quartz composite to sulfate groups was compared with activated carbon and anionic exchanger, where the concentration of sulfate group decreased from 131.67 to 5.62 ppm.

Carbon related materials, such as activated carbon, carbon nanotubes, graphene, graphene oxides, are known to have a large surface area and have been investigated in wastewater treatment for decades.[89–95] A combination of polyaniline and

carbon related materials are supposed to enhance the adsorption abilities.

Hierarchical nanocomposites of polyaniline (PANI) nanorods array on graphene oxide (GO) nanosheets were successfully generated by chemical oxidation polymerization in dilute solution under $-20\ °C$, as illustrated in Fig. 8. The removal of Cr(vɪ) by PANI/graphene oxide exhibited a superb capacity of 1149.4 mg g^{-1}.[48] This high capacity was due to the strong binding affinities of oxygen and nitrogen-containing functional groups on the PANI/graphene oxide surface, as characterized by AFM, TEM and SEM in Fig. 9. Bare graphene oxide can easily agglomerate to form a 2D nanosheet morphology. After decorated with PANI, the graphene oxide surface was covered by PANI nanorods uniformly, forming a rough surface and a free-standing sheet-like morphology of PANI/graphene oxide composite.

The adsorption capacities of PANI/graphene oxide nanocomposites were screened by the contact time, different ratios of aniline to graphene oxide, pH value effects and the adsorption isotherm (Fig. 10a–c). The maximum capacity condition can be reached at the longest contact time of 200 min for PANI/graphene oxide, the best mass ratio of aniline to graphene oxide at about 9.3 : 1 and an optimal pH around 2.0–3.0. The high removal efficiency at low pH values was reasoned as the strong electrostatic interactions between the protonated PANI surface and the negatively charged major species of $HCrO_4^-$. The adsorption isotherm (Fig. 10d) fitted well with Langmuir isotherm model with a calculated maximum adsorption capacity to be 1149.4 mg g^{-1}, which is the highest capacity as compared with other polymer based adsorbents (Fig. 10e, Table 6). Besides, the adsorption capacity had no obvious reduction even after seven adsorption/desorption cycles (Fig. 10f).

The adsorption of U(vɪ), Eu(ɪɪɪ), Sr(ɪɪ), and Cs(ɪ) was also investigated by PANI/graphene oxide, which followed the Langmuir isotherm model with maximum capacities to be 1.03, 1.65, 1.68, and 1.39 mmol g^{-1}, respectively.[96]

The magnetic PANI/carbon nanotube composite was prepared by plasma induced polymerization technique (Fig. 11). An enhanced adsorption ability was observed for Pb(ɪɪ)

Fig. 7 Proposed anionic exchange of AuI_2^- with Cl^- for AuI_2^- adsorption. Reprinted from ref. 88 with the permission from Wiley InterScience (2009).

Fig. 8 Schematic illustration the growth mechanism of PANI/graphene oxide. Reprinted from ref. 48 with the permission from The Royal Society of Chemistry (2013).
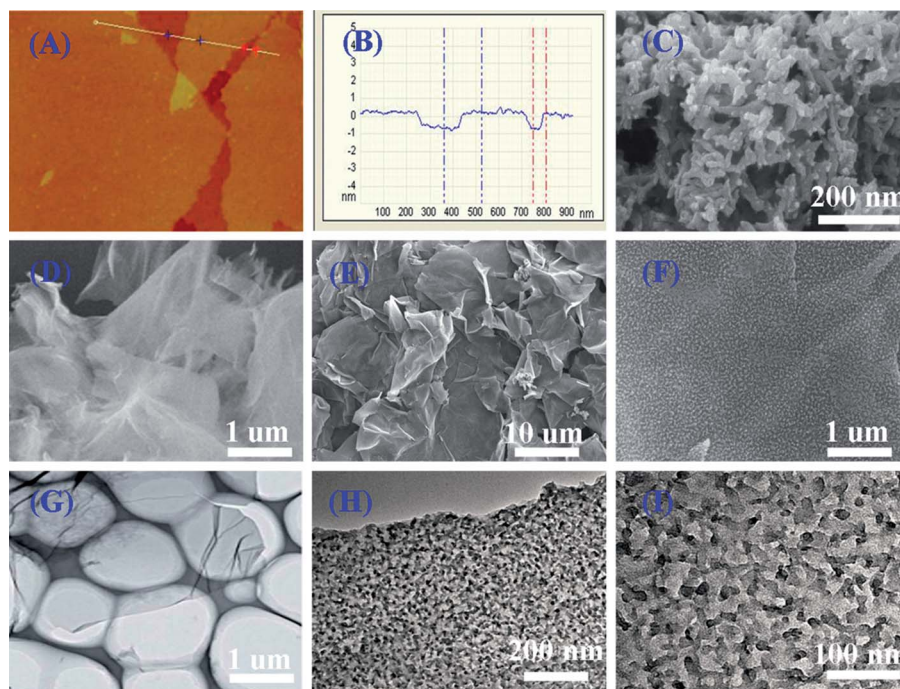
Fig. 9 AFM images of graphene oxide (a and b), SEM images of bare PANI (c), graphene oxide (d), PANI/graphene oxide composites (e and f), TEM images of bare graphene oxide (g), and PANI/graphene oxide composites (h and i). Reprinted from ref. 48 with the permission from The Royal Society of Chemistry (2013).

adsorption with a maximum capacity of 22.2 mg g^{-1}, which was attributed to the amine and imine functional groups.[97] After adsorption, the magnetic PANI/carbon nanotube composite can be easily separated and recovered by magnetic separation from aqueous solutions. A similar PANI/carbon nanotube composite was also applied for malachite green removal with the equilibrium adsorption amount and removal ratio to be 13.95 mg g^{-1} and 88%, respectively.[98]

Doping dodecyl-benzene-sulfonic-acid (DBSA) into PANI/carbon nanotube composite led to the PANI/carbon nanotube–DBSA nanocomposite.[100] The preparation, as well as the Cr(VI) adsorption, is depicted in Fig. 12 with a pseudo-second order kinetics, the Freundlich isotherm model and a maximum monolayer adsorption capacity of 55.55 mg g^{-1}. Electrostatic interactions between PANI and Cr(VI) anions were the predominant driving forces for this adsorption process. Desorption efficiency increases with increasing concentration of NaOH solution. However, only 20.77% Cr(VI) can be desorbed by 1.0 M NaOH solution, which may be attributed to the strong chemical bond formed between Cr(VI) and amino/imine groups of polyaniline and/or the adsorption of Cr(VI) into porous carbon nanotube.

Granular activated carbon was modified by polyaniline to prepare PANI/activated carbon composite, which reduced arsenate concentration from 120–1910 ppb to less than 10 ppb by reducing the arsenate to arsenite.[101]

Moreover, a variety of other PANI/organic composites were investigated in wastewater purifications. Examples involved the Congo red[64] and Cr(VI)[63] removal by PANI/PPy composite, PANI/humic acid for Hg(II) adsorption with a maximum capacity of

671 mg g^{-1},[65] Zn(II) by PANI/rice husk nanocomposite with a monolayer adsorption of 24.3 mg g^{-1},[102] and *p*-toluenesulfonic acid or camphorsulfonic acid doped PANI for the adsorption of various cationic and anionic dyes, such as orange-G, methylene blue, malachite green, rhodamine B, Alizarine cyanine green, Coomassie brilliant blue R-250 and so on.[103]

4. PPy related composites in water purification

Polypyrrole (PPy) is one of the most extensively studied conductive polymers because of the unique properties of pyrrole monomers, such as easy oxidization, water solubility, commercial availability, environmental stability, good redox property and high electrical conductivity.[104] The first examples of PPy were reported in 1963 as a highly conductive material by Weiss and coworkers.[105]

Due to the high conductivity, thermal and environmental stability and relative easy synthesis, the as-prepared PPy had been applied as biosensors, antistatic coatings, microactuators, functional membranes, *etc.* The adsorption abilities in wastewater purification were also investigated because of the abundant amino groups, which can interact with organic and inorganic molecules, such as Cr(VI),[55] Cu(II)[106] and pyrrole monomers.[107] However, the widely application as adsorbents was limited by its poor mechanical strength, low processability, and particularly the insolubility in common solvents. The improvement to these properties can be achieved either by forming copolymers or by fabricating PPy composites or blends

Fig. 10 The effect of contact time on Cr(vi) removal (a), the Cr(vi) removal capacity by PANO/graphene oxide nanocomposites synthesized by different mass ratios of aniline to graphene oxide (b), the effect of pH on Cr(vi) removal (c), the adsorption isotherm for Cr(vi) removal (d), comparison of Cr(vi) with other polymer adsorbents (e) and seven cycles of Cr(vi) adsorption capacity by PANI/graphene oxide nanocomposites (f). Reprinted from ref. 48 with the permission from The Royal Society of Chemistry (2013).

Table 6 Comparison of adsorption capacity of PPy/graphene oxide with other adsorbents for Cr(vi) removal

Adsorbents	q_m (mg g^{-1})	Equilibrium time (h)	Optimum pH	Ref.
PANI nanorods/graphene oxide nanosheets	1149.4	2.67	3.0	48
PPy/wood sawdust	3.4	0.16	5.0	52
PPy/PANI nanofibers	227	3.0	2.0	63
PPy/Fe$_3$O$_4$ magnetic nanocomposite	243.9	3.0	2.0	67
1D PANI nanowire/tubes	84.8	1.0	5.0	72
PANI/montmorillonite nanocomposite	167.5	1.0	2.0	81
Poly(N-methylaniline)/chitosan composite	192.4	—	4.2	86
Poly(2-ethylaniline)/chitosan composite	148.7	—	4.2	86
Poly(N-ethylaniline)/chitosan composite	229.8	—	4.2	86
PANI/carbon nanotube-DBSA nanocomposite	55.55	10	2.0	100
PPy/Fe$_3$O$_4$ nanocomposite	237.17	—	2.0	108
Orange-like Fe$_3$O$_4$/PPy composite microspheres	209.2	12	2.0	110
PPy/montmorillonite clay composite	119.34	—	2.0	113
PPy/graphene oxide composite nanosheets	497.1	24	3.0	124

Fig. 11 The equipment of plasma induced reaction and the reaction mechanism. Reprinted from ref. 99 with permission from WILEY-VCH Verlag GmbH & Co. KGaA, Weinheim (2010).
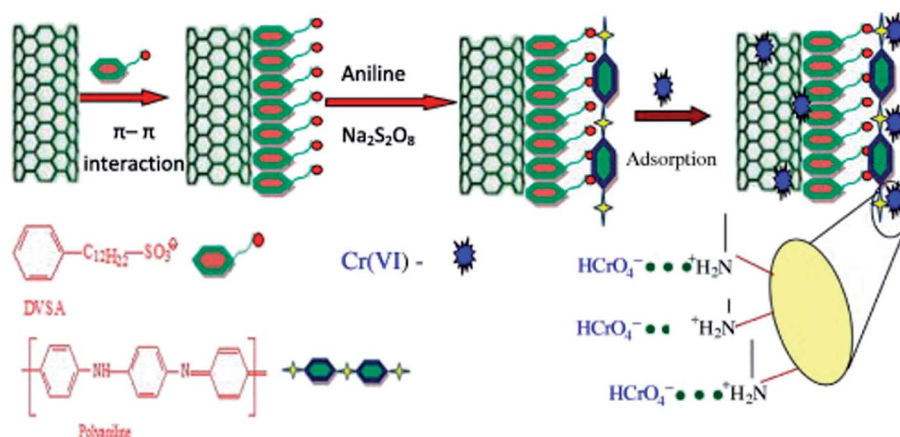

Fig. 12 Schematic representation of PANI/carbon nanotube−DBSA nanocomposite preparation and Cr(vi) adsorption. Reprinted from ref. 100 with the permission from Elsevier (2013).

with other functional materials, such as sawdust, rice husk ash, magnetic Fe_3O_4, carbon nanotubes, graphene oxides, polysaccharides, and so on. The modified PPy composites or blends can also be divided into PPy/inorganic material composites and PPy/organic material composites, depending on the nature of the incorporating functional materials.

4.1 PPy/inorganic composites

Magnetic Fe_3O_4 is widely doped with PPy to fabricate PPy/magnetic Fe_3O_4 composite for wastewater treatment, thanks to the advantage of easy magnetic separation of the composite from aqueous solution. The pollutants involved $HCrO_4^-$,[67,108] $K_2Cr_2O_7$ (ref. 109 and 110) and F^-.[68] Onyango group carried out a comprehensive investigation toward the Cr(vi) removal.[67,108] PPy was coated on magnetic Fe_3O_4 *via in situ* chemical oxidation by $FeCl_3$. The SEM images of Fe_3O_4 and PPy/magnetic Fe_3O_4 composite, as well as TEM image of PPy/magnetic Fe_3O_4 composite, were collected in Fig. 13. Fe_3O_4 nanoparticles were agglomerated because of the high surface area and magneto dipole–dipole interactions between Fe_3O_4 particles (Fig. 12a).

Fig. 13 SEM images of Fe_3O_4 particles (a) and PPy/magnetic Fe_3O_4 composite (b), and TEM image of PPy/magnetic Fe_3O_4 composite. Reprinted from ref. 108 with permission from Elsevier (2013).

The PPy/magnetic Fe_3O_4 composite had larger size after precipitating PPy moieties onto Fe_3O_4 particles with a core–shell structure. The as-prepared PPy/magnetic Fe_3O_4 composite can almost quantitatively remove Cr(VI) with a 200 mg L^{-1} Cr(VI) aqueous solution at pH 2.0 (Fig. 14a). The adsorption process was spontaneous and endothermic, and followed a pseudo-second order kinetic model (Fig. 14b–d). The mechanism involved the Langmuir isotherm model and an ionic exchange process (Fig. 14e and f). Compared with quantitative removal efficiency of Cr(VI), only 14% of the adsorbed Cr(VI) was

Fig. 14 Effect of pH (a), plot to determine thermodynamic parameters (b), pseudo-first-order (c), pseudo-second-order (d), Langmuir isotherm model (e) and Freundlich isotherm model (f) of Cr(VI) removal by PPy/Fe₃O₄ nanocomposites. Reprinted from ref. 67 with permission from Elsevier (2011).

desorbed by 0.5 M NaOH solution. A further treatment with 2.0 M HCl solution could desorb the rest reduced Cr(III). The original adsorption capacity can maintain for at least two recycles.

Fig. 15   SEM images of sawdust (left) and PPy/sawdust composite (right). Reprinted from ref. 69 with permission from Elsevier (2012).
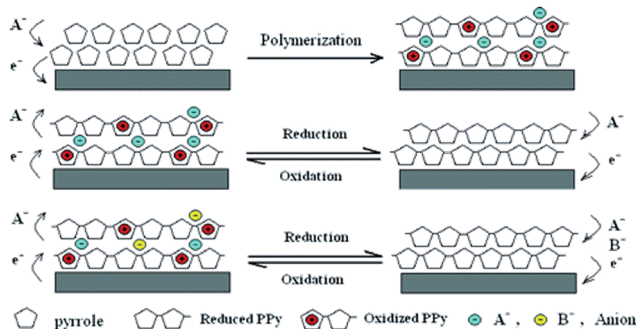

Fig. 16   Schematic illustration for the polymerization of PPy and the anion exchange process. Reprinted from ref. 120 with the permission from American Chemical Society (2006).

Fe_3O_4 can also serve as an oxidant for PPy/Fe_3O_4 nanoclusters fabrication as reported by Cui group.[109] The as-synthesized PPy/Fe_3O_4 nanoclusters demonstrated a maximum $K_2Cr_2O_7$ removal ability of 3.47 mmol g^{-1} at pH 5.0, which was much higher than PPy and activated carbon composite.

Other PPy/inorganic composites involved the removal of humic acid by PPy/glass beads composite,[111] adsorption of polyoxometalate $SiMo_{12}O_{40}^{4-}$ by PPy/In_2O_3 composite,[112] Cr(VI) removal by PPy/montmorillonite clay composite,[113] and the PPy/Al_2O_3 composite for Cd(II) removal.[114]

4.2   PPy/organic composites

Compared with limited PPy/inorganic composites, a variety of organic materials were combined with PPy, which included sawdust, polysaccharides, carbon related nanomaterials, rice husk ash, *etc.* This can be attributed to the natural compatibility and the easy covalent bonding abilities of PPy.

PPy/sawdust composites were synthesized by *in situ* FeCl$_3$ oxidation and had applied to remove Cr(VI),[52] Zn(II),[53] phosphate,[51] nitrate,[69] carmoisine,[49] and methylene blue.[50] All the adsorption processes were spontaneous and obeyed the pseudo-second order kinetics. The adsorption of Cr(VI), Zn(II) and nitrate followed the Freundlich isotherm model, and the phosphate, carmoisine and methylene removal fitted with Langmuir isotherm model. The surface morphology change was illustrated in Fig. 15. PPy particles were coated both outside surface and inside of the sawdust, forming a uniform morphology with increased surface area and adsorption ability.

Fig. 17   The Cr(VI) removal capacity of PPy/graphene oxide *versus* PPy (a), linear correlation to Langmuir isotherm model (b), the Cr(VI) removal capacity of PPy/graphene oxide with different Cr(VI) initial concentration (c) and the pseudo-second order model for Cr(VI) adsorption by PPy/graphene oxide nanocomposite. Reprinted from ref. 124 with the permission from PLOS One (2012).

Cellulose acetate membrane[115] and cellulose fiber[116] were coated on PPy to remove gold iodide and Cr(vi), respectively. Ionic exchange was ascribed for gold iodide removal and the reduction of Cr(vi) to Cr(iii). A covalently immobilized heparin–PPy/poly(ethylene glycol) methacrylate composite was also fabricated for biological applications to reduce the protein and thrombus formation.[117]

Similar to PANI, the carbon related materials, activated carbon, carbon nanotube and graphene oxide, were also doped with PPy to fabricate PPy/carbon related composites for wastewater treatment. PPy/impregnated porous carbon was prepared by vapor infiltration polymerization technique to obtain a mesoporous structure.[118] The as-prepared composite exhibited an improved adsorption ability to remove heavy metal ions, such as Hg(ii), Pb(ii) and Ag(i) due to the amino groups of PPy. PPy/carbon nanotube composites can be prepared by grafting from technique either chemically or electrochemically. The chemical fabricated PPy/carbon nanotube composite can effectively remove heavy metals, anions and chemical oxygen demand from paper mill waste.[119] The electrochemical

synthesized PPy/carbon nanotube provided a simple and highly effective method for ClO_4^- removal *via* electrically switched ion exchange technique (Fig. 16).[120]

The PPy/reduced graphene oxide composite was also investigated to remove Hg(ii),[121,122] Pb(ii)[123] and Cr(vi).[124] The chemical oxidation polymerized PPy/reduced graphene oxide composites showed a higher selective Hg(ii) removal capacity, as compared with Pb(ii), Cd(ii), Zn(ii), and Cu(ii) from aqueous solutions, as well as a high desorption capacity of up to 92.3%.[121] The same composites were synthesized from a electrochemical polymerization methods, which exhibited a similar selectivity to detect Hg(ii).[122]

The removal of Cr(vi) by PPy/graphene oxide nanosheets were produced by sacrificial-template polymerization, utilizing MnO_2 nanoslices as both the sacrificial-template and the oxidant.[124] The as-prepared PPy/graphene oxide nanocomposites exhibited a doubled adsorption capacity than the conventional PPy nanoparticles. The color change from light yellow to almost transparent further confirmed the adsorption of Cr(vi), as shown in Fig. 17a. The effect of the Cr(vi) initial concentration
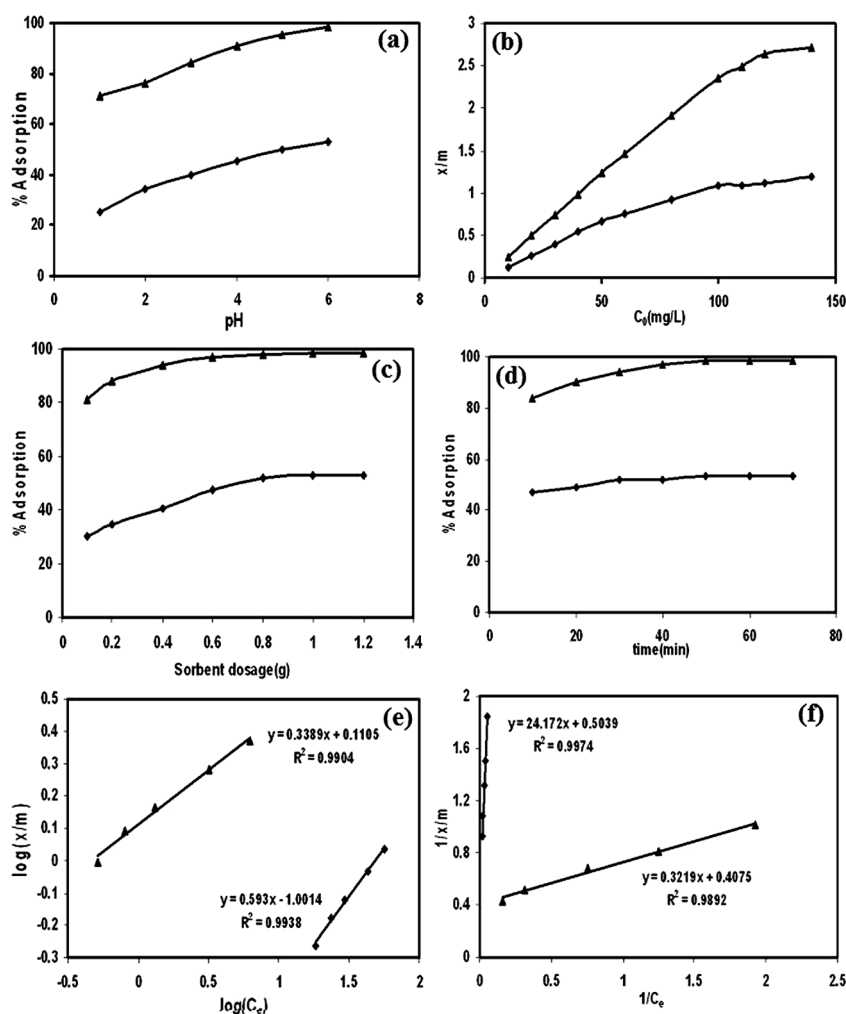

Fig. 18 The influencing factors of pH (a), initial concentration (b), sorbent dosage (c), contact time (d), the Freundlich isotherm (e) and the Langmuir isotherm (f) of Ag(i) adsorption by sawdust (■) and poly(3-methyl thiophene)/sawdust composite (▲). Reprinted from ref. 131 with permission from Wiley InterScience (2009).

on Cr(VI) removal by the PPy/graphene oxide was screened from 0.38 mmol L^{-1} to 1.97 mmol L^{-1}. With increasing the Cr(VI) initial concentration, longer equilibrium time was required, as well as decreased adsorption efficiency, which might due to the rigorous competition for the adsorption sites (Fig. 17c). This adsorption process fitted well with Langmuir isotherm model and obeyed the pseudo-second-order kinetics (Fig. 17b and d). The maximum adsorption capacity was calculated to be 497.1 mg g^{-1}, which is much higher than most of the other nano-composites (Table 6).

Eisazadeh group fabricated PPy/rice husk ash composites to remove a variety of inorganic ions from aquatic environments, such as Zn, Fe, Cu, Mn, Cl$^-$, S^{2-}, SO$_3^{2-}$ and so on.[125,126] Electropolymerized PPy/SDBS composite was applied to remove bovine serum albumin and fibrinogen.[127] PPy/nylon 6,6 granules can adsorb humic acid from aqueous solutions and regenerate by washing with 1.0 M NaOH, 1.0 M HCl solution and distilled water consecutively.[128] Pb(II), Cd(II) and Ni(II) can be enriched by PPy/melanine or PPy/poly(styrene-sulfate) composites.[129]

5. Miscellaneous conjugated polymer composites in water purification

Polythiophenes (PT) are stable in their oxidized and neutral states. The ease of substitutions at the third position can produce versatile modified PT with different stability, solubility and conductivity. Compared with PANI and PPy, PTs have even lower solubility in common solvents, which call for the incorporation of other functional materials to fabricate PTs composites for water purification.

Poly(3-methyl thiophene)/sawdust was fabricated by *in situ* chemical oxidation with FeCl$_3$ to remove methylene blue. The adsorption capacity can reach 191 mg g^{-1}, which was seven times higher than sawdust.[130] The increased surface area may be ascribed to the high adsorption capacity, as observed from the change of surface morphology. Sawdust had a smooth surface and layer structure, while poly(3-methyl thiophene)/sawdust composite had heterogeneous morphology with porous surface area. The adsorbed dyes can be desorbed by washing with 0.10 M HCl/ethanol solution, and the adsorption efficiency remained 93% after three recycles.

The same composite was also applied in Ag(I) removal from aqueous solution.[131] The influencing factors, including pH, initial concentration, sorbent dosage and exposure time, on Ag(I) removal were investigated (Fig. 18). The sorption efficiency was proportional to the increasing pH values, initial concentration, sorbent dosage and the contact time. The sorption isotherm indicated that both the Langmuir isotherm and the Freundlich isotherms can be applied in this system. Desorption studies revealed that the maximum recovery can reach 40% and 42% by 0.5 HNO$_3$ and 1.0 M ammonia solutions, respectively.

Different poly(alky-substituted thiophene)/polytetrafluoroethylene composites were produced by emulsion polymerization.[132] The as-prepared composites can effectively adsorb protein. A two-layer composite of polystyrene and PT was prepared to reduce the protein and bacterial cell adsorptions.[133]

Other conjugated polymers, such as polyacetylenes, poly-(phenylenevinylene) (PPV), poly(*p*-phenylene) (PPP), *etc.*, may also be applied as composites in wastewater treatment. However, due to the lack of heteroatoms for the functional group interactions with pollutants, their practical applications are still not reported yet.

6. Conclusion

Current investigations indicated the successful removal of various pollutants from aqueous solution by versatile conjugated polymer based composites. Different composites exhibited different selectivities to adsorb diverse pollutants, ranging from inorganic heavy metals to organic aromatic molecules. One noticeable problem is that current composites are only effective to a narrow range of pollutants, thus, new composites that are capable of removing more broad spectrum of pollutants are highly required since wastewater usually contains multiple pollutants. The practical applications are also impeded by other factors, such as the overall adsorption efficiency, economic issue, adsorption/desorption efficiency, and so on, which call for the development of new cost-effective and high efficient composites for large scale applications.

We have reviewed the conjugated polymer based composites that are often fabricated from the easy-prepared functionalized materials with unique surface modifications. However, compared with the extensive and delicate fabrication of counterpart composites used in conducting material studies, the discussed composites (*i.e.*, PANI, PPy and PT) are far less developed, which are mainly sourced by blending with limited inorganic materials (*i.e.*, silica and Fe$_3$O$_4$) or organic materials (cellulose, activated carbon, carbon nanotube and graphene/graphene oxide). More types of novel composites are required for new applications in wastewater purification, such as poly/clay composite, which is a promising type of composite with multiple microstructures.

The morphologies of the discussed composites are not well controlled, which may limit the surface area for the maximum pollutant adsorption. Future research to fabricate precise and delicate controlled composite morphology is desirable. For example, hollow fiber materials can be blended with current polymers to fabricate composites with high specific surface area and tough self-hold structure.

The composites discussed in this review were predominantly produced by physical blending with few covalent bonded polymers. More efforts are required to make covalent bonded composites. One recommendation involves the cross-linking chemistry. Cross-linking is a simple and effective modification method to improve the plasticisation resistance, stability of composites to stand harsh conditions. More importantly, this technique can fabricate both structural and morphological homogenous composites to improve the adsorption capacities. Moreover, theoretical investigation in water purification is also needed. Theoretical investigations

to the adsorption mechanism and kinetics can also provide useful guidance to design and optimize composite fabrication.

Acknowledgements

References

1 http://www.worldbank.org/en/topic/water/overview.

2 http://www.unwater.org/statistics/statistics-detail/en/c/211794/.

3 M. Ayad and S. Zaghlol, *Chem. Eng. J.*, 2012, **204–206**, 79–86.

4 M. Ayad, G. El-Hefnawy and S. Zaghlol, *Chem. Eng. J.*, 2013, **217**, 460–465.

5 J. Wang, K. Zhang and L. Zhao, *Chem. Eng. J.*, 2014, **239**, 123–131.

6 S. Ding, C. Zheng and J. Wang, Adsorption of Aqueous Cr(VI) on Polyaniline: Adsorption Isotherms and Adsorption Kinetics, *Conference on Environmental Pollution and Public Health (CEPPH 2010 E-BOOK)*, Wuhan, China, 2010.

7 S. K. Bajpai and M. Bhowmik, *J. Appl. Polym. Sci.*, 2010, **117**, 3615–3622.

8 H.-J. Lee, B. Doo Chin, S.-M. Yang and O. O. Park, *J. Colloid Interface Sci.*, 1998, **206**, 424–438.

9 D. Mahanta, G. Madras, S. Radhakrishnan and S. Patil, *J. Phys. Chem. B*, 2008, **112**, 10153–10157.

10 N. V. Blinova, J. Stejskal, J. M. Fréchet and F. Svec, *J. Polym. Sci., Part A: Polym. Chem.*, 2012, **50**, 3077–3085.

11 J. Yan, T. Wei, B. Shao, Z. Fan, W. Qian, M. Zhang and F. Wei, *Carbon*, 2010, **48**, 487–493.

12 M. S. Mansour, M. E. Ossman and H. A. Farag, *Desalination*, 2011, **272**, 301–305.

13 R. Ansari and H. Dezhampanah, *Eur. Chem. Bull.*, 2013, **2**, 220–225.

14 J. Sudha, S. Sivakala, C. Chandrakanth, K. Neethu, K. Rohini and R. Ramakrishnan, *eXPRESS Polym. Lett.*, 2014, **8**, 107–115.

15 G. Korotcenkov, in *Handbook of Gas Sensor Materials*, Springer, New York, 2014, ch. 8, pp. 131–146, DOI: 10.1007/978-1-4614-7388-6_8.

16 M. Naushad, Z. AL-Othman and M. Islam, *Int. J. Environ. Sci. Technol.*, 2013, 1–12.

17 M. Bajpai, N. Rai and S. K. Bajpai, *J. Appl. Polym. Sci.*, 2012, **125**, 1382–1390.

18 J. Yan, T. Wei, Z. Fan, W. Qian, M. Zhang, X. Shen and F. Wei, *J. Power Sources*, 2010, **195**, 3041–3045.

19 A. A. Shyaa, O. A. Hasan and A. M. Abbas, *J. Saudi Chem. Soc.*, 2012, DOI: doi:10.1016/j.jscs.2012.01.001.

20 Y. Liao, C. Zhang, Y. Zhang, V. Strong, J. Tang, X.-G. Li, K. Kalantar-Zadeh, E. M. Hoek, K. L. Wang and R. B. Kaner, *Nano Lett.*, 2011, **11**, 954–959.

21 M. Ghorbani, M. S. Lashkenari and H. Eisazadeh, *Synth. Met.*, 2011, **161**, 1430–1433.

22 C. Dhand, M. Das, M. Datta and B. D. Malhotra, *Biosens. Bioelectron.*, 2011, **26**, 2811–2821.

23 M. Trchová, Z. Morávková, I. Šeděnková and J. Stejskal, *Chem. Pap.*, 2012, **66**, 415–445.

24 R. Gangopadhyay and A. De, *Chem. Mater.*, 2000, **12**, 608–622.

25 L. Wang, X. Lu, S. Lei and Y. Song, *J. Mater. Chem. A*, 2014, **2**, 4491–4509.

26 G. Ćirić-Marjanović, in *Nanostructured Conductive Polymers*, John Wiley & Sons, Ltd, 2010, ch. 2, pp. 19–98, DOI: 10.1002/9780470661338.

27 R. Y. Suckeveriene, E. Zelikman, G. Mechrez and M. Narkis, *Rev. Chem. Eng.*, 2011, **27**, 15–21.

28 A. J. Heeger, *Rev. Mod. Phys.*, 2001, **73**, 681–700.

29 A. A. Syed and M. K. Dinesan, *Talanta*, 1991, **38**, 815–837.

30 A. G. MacDiarmid, *Synth. Met.*, 1997, **84**, 27–34.

31 M. Omastová and M. Mičušík, *Chem. Pap.*, 2012, **66**, 392–414.

32 D. D. Ateh, H. A. Navsaria and P. Vadgama, *J. R. Soc., Interface*, 2006, **3**, 741–752.

33 V. V. Tat'yana and N. E. Oleg, *Russ. Chem. Rev.*, 1997, **66**, 443.

34 I. F. Perepichka and D. F. Perepichka, *Handbook of thiophene-based materials: applications in organic electronics and photonics*, Wiley Online Library, 2009.

35 R. D. McCullough, *Adv. Mater.*, 1998, **10**, 93–116.

36 C. Zanardi, F. Terzi and R. Seeber, *Anal. Bioanal. Chem.*, 2013, **405**, 509–531.

37 R. S. Bobade, *J. Polym. Eng.*, 2011, **31**, 209–215.

38 H.-J. Wang, C.-P. Chen and R.-J. Jeng, *Materials*, 2014, **7**, 2411–2439.

39 K. R. Hall, L. C. Eagleton, A. Acrivos and T. Vermeulen, *Ind. Eng. Chem. Fundam.*, 1966, **5**, 212–223.

40 I. Langmuir, *J. Am. Chem. Soc.*, 1918, **40**, 1361–1403.

41 J. Wang, X. Han, H. Ma, Y. Ji and L. Bi, *Chem. Eng. J.*, 2011, **173**, 171–177.

42 H. M. F. Freundlich, *Z. Phys. Chem.*, 1906, **57A**, 385–470.

43 C. Lu, Y.-L. Chung and K.-F. Chang, *J. Hazard. Mater.*, 2006, **138**, 304–310.

44 F. Sánchez Rojas and C. Bosch Ojeda, *Anal. Chim. Acta*, 2009, **635**, 22–44.

45 M. Dubinin, *Chem. Rev.*, 1960, **60**, 235–241.

46 M. Temkin and V. Pyzhev, *Acta Physicochim. URSS*, 1940, **12**, 217–222.

47 F. Kanwal, R. Rehman, T. Mahmud, J. Anwar and R. Ilyas, *J. Chil. Chem. Soc.*, 2012, **57**, 1058–1063.

48 S. Zhang, W. Xu, J. Li, J. Li, J. Xu and X.-K. Wang, *Dalton Trans.*, 2013, **42**, 7854–7858.

49 R. Ansari, M. B. Keivani and A. F. Delavar, *J. Appl. Polym. Sci.*, 2011, **122**, 804–812.

50 R. Ansari and Z. Mosayebzadeh, *J. Iran. Chem. Soc.*, 2010, **7**, 339–350.

51 S. K. Bajpai, V. K. Rohit and M. Namdeo, *J. Appl. Polym. Sci.*, 2009, **111**, 3081–3088.

52 R. Ansari and N. K. Fahim, *React. Funct. Polym.*, 2007, **67**, 367–374.

53 M. Omraei, H. Esfandian, R. Katal and M. Ghorbani, *Desalination*, 2011, **271**, 248–256.

54 M. Karthikeyan, K. K. Satheeshkumar and K. P. Elango, *J. Hazard. Mater.*, 2009, **167**, 300–305.

55 R. Katal, M. Ghiass and H. Esfandian, *J. Vinyl Addit. Technol.*, 2011, **17**, 222–230.

56 M. Özacar, İ. A. Şengil and H. Türkmenler, *Chem. Eng. J.*, 2008, **143**, 32–42.

57 Y.-S. Ho and G. McKay, *Process Biochem.*, 1999, **34**, 451–465.

58 S. H. Chien and W. R. Clayton, *Soil Sci. Soc. Am. J.*, 1980, **44**, 265–268.

59 Y.-S. Ho, *Water Res.*, 2006, **40**, 119–125.

60 Y. S. Ho, *Pol. J. Environ. Stud.*, 2006, **15**, 81–86.

61 B. Royer, N. F. Cardoso, E. C. Lima, J. C. P. Vaghetti, N. M. Simon, T. Calvete and R. C. Veses, *J. Hazard. Mater.*, 2009, **164**, 1213–1222.

62 M. M. Ayad, A. Abu El-Nasr and J. Stejskal, *J. Ind. Eng. Chem.*, 2012, **18**, 1964–1969.

63 M. Bhaumik, A. Maity, V. V. Srinivasu and M. S. Onyango, *Chem. Eng. J.*, 2012, **181**, 323–333.

64 M. Bhaumik, R. McCrindle and A. Maity, *Chem. Eng. J.*, 2013, **228**, 506–515.

65 Y. Zhang, Q. Li, L. Sun, R. Tang and J. P. Zhai, *J. Hazard. Mater.*, 2010, **175**, 404–409.

66 V. Janaki, K. Vijayaraghavan, A. K. Ramasamy, K. J. Lee, B. T. Oh and S. Kamala-Kannan, *J. Hazard. Mater.*, 2012, **241**, 110–117.

67 M. Bhaumik, A. Maity, V. V. Srinivasu and M. S. Onyango, *J. Hazard. Mater.*, 2011, **190**, 381–390.

68 M. Bhaumik, T. Y. Leswifi, A. Maity, V. V. Srinivasu and M. S. Onyango, *J. Hazard. Mater.*, 2011, **186**, 150–159.

69 H. Pahlavanzadeh, R. Katal and H. Mohammadi, *J. Ind. Eng. Chem.*, 2012, **18**, 948–956.

70 Z. A. Al-Othman, Inamuddin and M. Naushad, *Chem. Eng. J.*, 2011, **169**, 38–42.

71 J. Wang, B. L. Deng, H. Chen, X. R. Wang and J. Z. Zheng, *Environ. Sci. Technol.*, 2009, **43**, 5223–5228.

72 X. A. Guo, G. T. Fei, H. Su and L. D. Zhang, *J. Phys. Chem. C*, 2011, **115**, 1608–1613.

73 F. Belaib, A. H. Meniai and M. B. Lehocine, *Energy Procedia*, 2012, **18**, 1254–1260.

74 M. M. Ayad and A. A. El-Nasr, *J. Nanostructure Chem.*, 2012, **3**, 1–9.

75 M. B. Gholivand and M. M. Abolghasemi, *J. Sep. Sci.*, 2012, **35**, 695–701.

76 A. Mehdinia, M. Ahmadifar, M. O. Aziz-Zanjani, A. Jabbari and M. S. Hashtroudi, *Analyst*, 2012, **137**, 4368–4374.

77 H. Javadian, P. Vahedian and M. Toosi, *Appl. Surf. Sci.*, 2013, **284**, 13–22.

78 J. M. Pan, H. Yao, W. Guan, H. X. Ou, P. W. Huo, X. Wang, X. H. Zou and C. X. Li, *Chem. Eng. J.*, 2011, **172**, 847–855.

79 R. Katal, S. Pourkarimi, E. Bahmani, H. A. Dehkordi, M. A. Ghayyem and H. Esfandian, *J. Vinyl Addit. Technol.*, 2013, **19**, 147–156.

80 U. Ozdemir, B. Ozbay, S. Veli and S. Zor, *Chem. Eng. J.*, 2011, **178**, 183–190.

81 J. Chen, X. Q. Hong, Y. T. Zhao, Y. Y. Xia, D. K. Li and Q. F. Zhang, *J. Mater. Sci.*, 2013, **48**, 7708–7717.

82 H. Cui, Y. Qian, Q. Li, Q. Zhang and J. P. Zhai, *Chem. Eng. J.*, 2012, **211**, 216–223.

83 P. Xiong, Q. Chen, M. He, X. Sun and X. Wang, *J. Mater. Chem.*, 2012, **22**, 17485–17493.

84 D. L. Liu and D. Z. Sun, *Environ. Eng. Sci.*, 2012, **29**, 461–465.

85 R. Ansari, *Acta Chim. Slov.*, 2006, **53**, 88.

86 A. G. Yavuz, E. Dincturk-Atalay, A. Uygun, F. Gode and E. Aslan, *Desalination*, 2011, **279**, 325–331.

87 F. Rodriguez, M. M. Castillo-Ortega, J. C. Encinas, H. Grijalva, F. Brown, V. M. Sanchez-Corrales and V. M. Castano, *J. Appl. Polym. Sci.*, 2009, **111**, 1216–1224.

88 F. Rodriguez, M. M. Castillo-Ortega, J. C. Encinas, V. M. Sanchez-Corrales, M. Perez-Tello and G. T. Munive, *J. Appl. Polym. Sci.*, 2009, **113**, 2670–2674.

89 T. J. Bandosz, *Activated carbon surfaces in environmental remediation*, Academic Press, 1st edn, 2006.

90 R. C. Bansal and M. Goyal, *Activated carbon adsorption*, CRC press, 2010.

91 F. Çeçen and Ö. Akta, *Activated carbon for water and wastewater treatment: Integration of adsorption and biological treatment*, Wiley-VCH Verlag GmbH & Co. KGaA, 2011.

92 J. Jang, in *Emissive Materials Nanomaterials*, Springer, 2006, pp. 189–260.

93 X. Liu, M. Wang, S. Zhang and B. Pan, *J. Environ. Sci.*, 2013, **25**, 1263–1280.

94 M. Meyyappan, *Carbon nanotubes: science and applications*, CRC press, 2004.

95 V. K. K. Upadhyayula, S. G. Deng, M. C. Mitchell and G. B. Smith, *Sci. Total Environ.*, 2009, **408**, 1–13.

96 Y. Sun, D. Shao, C. Chen, S. Yang and X. Wang, *Environ. Sci. Technol.*, 2013, **47**, 9904–9910.

97 D. D. Shao, C. L. Chen and X. K. Wang, *Chem. Eng. J.*, 2012, **185**, 144–150.

98 Y. Zeng, L. J. Zhao, W. D. Wu, G. X. Lu, F. Xu, Y. Tong, W. B. Liu and J. H. Du, *J. Appl. Polym. Sci.*, 2013, **127**, 2475–2482.

99 D. D. Shao, Z. Q. Jiang and X. K. Wang, *Plasma Processes Polym.*, 2010, **7**, 552–560.

100 R. Kumar, M. O. Ansari and M. A. Barakat, *Chem. Eng. J.*, 2013, **228**, 748–755.

101 L. Yang, S. N. Wu and J. P. Chen, *Ind. Eng. Chem. Res.*, 2007, **46**, 2133–2140.

102 M. Ghorbani, H. Eisazadeh and A. Ghoreyshi, *Iran. J. Energy Environ.*, 2012, **3**, 66–71.

103 D. Mahanta, G. Madras, S. Radhakrishnan and S. Patil, *J. Phys. Chem. B*, 2009, **113**, 2293–2299.

104 A. Kassim, Z. B. Basar and H. E. Mahmud, *J. Chem. Sci.*, 2002, **114**, 155–162.

105 R. McNeill, R. Siudak, J. Wardlaw and D. Weiss, *Aust. J. Chem.*, 1963, **16**, 1056–1075.

106 C. M. S. Piatnicki, D. S. Azambuja, E. E. S. Hasse, K. R. L. Castagno and S. B. Guterres, *Sep. Sci. Technol.*, 2002, **37**, 2459–2476.

107 M. Marandi, S. Kallip, V. Sammelselg and J. Tamm, *Electrochem. Commun.*, 2010, **12**, 854–858.

108 M. Bhaumik, K. Setshedi, A. Maity and M. S. Onyango, *Sep. Purif. Technol.*, 2013, **110**, 11–19.

109 T. J. Yao, T. Y. Cui, J. Wu, Q. Z. Chen, S. W. Lu and K. N. Sun, *Polym. Chem.*, 2011, **2**, 2893–2899.

110 Y. Wang, B. Zou, T. Gao, X. Wu, S. Lou and S. Zhou, *J. Mater. Chem.*, 2012, **22**, 9034–9040.

111 R. B. Bai and X. Zhang, *J. Colloid Interface Sci.*, 2001, **243**, 52–60.

112 D. Martel, H. N. Cong, M. Molinari, J. Ebothe and I. V. Kityk, *J. Mater. Sci.*, 2008, **43**, 3486–3490.

113 K. Z. Setshedi, M. Bhaumik, S. Songwane, M. S. Onyango and A. Maity, *Chem. Eng. J.*, 2013, **222**, 186–197.

114 T. Hasani and H. Eisazadeh, *Synth. Met.*, 2013, **175**, 15–20.

115 M. M. Castillo-Ortega, I. Santos-Sauceda, J. C. Encinas, D. E. Rodriguez-Felix, T. del Castillo-Castro, F. Rodriguez-Felix, J. L. Valenzuela-Garcia, L. S. Quiroz-Castillo and P. J. Herrera-Franco, *J. Mater. Sci.*, 2011, **46**, 7466–7474.

116 Y. Lei, X. Qian, J. Shen and X. An, *Ind. Eng. Chem. Res.*, 2012, **51**, 10408–10415.

117 Y. L. Li, K. G. Neoh and E. T. Kang, *J. Colloid Interface Sci.*, 2004, **275**, 488–495.

118 M. Choi and J. Jang, *J. Colloid Interface Sci.*, 2008, **325**, 287–289.

119 M. Ghorbani and H. Eisazadeh, *J. Vinyl Addit. Technol.*, 2013, **19**, 213–218.

120 Y. H. Lin, X. L. Cui and J. Bontha, *Environ. Sci. Technol.*, 2006, **40**, 4004–4009.

121 V. Chandra and K. S. Kim, *Chem. Commun.*, 2011, **47**, 3942–3944.

122 Z.-Q. Zhao, X. Chen, Q. Yang, J.-H. Liu and X.-J. Huang, *Chem. Commun.*, 2012, **48**, 2180–2182.

123 Z.-Q. Zhao, X. Chen, Q. Yang, J.-H. Liu and X.-J. Huang, *Electrochem. Commun.*, 2012, **23**, 21–24.

124 S. K. Li, X. F. Lu, Y. P. Xue, J. Y. Lei, T. Zheng and C. Wang, *PLoS One*, 2012, **7**, e43328.

125 M. Ghorbani and H. Eisazadeh, *Synth. Met.*, 2012, **162**, 1429–1433.

126 M. Ghorbani and H. Eisazadeh, *Composites, Part B*, 2013, **45**, 1–7.

127 M. L. Liu, Y. Y. Zhang, M. L. Wang, C. Y. Deng, Q. J. Xie and S. Z. Yao, *Polymer*, 2006, **47**, 3372–3381.

128 X. Zhang and R. B. Bai, *J. Mater. Chem.*, 2002, **12**, 2733–2739.

129 M. Hepel, X. M. Zhang, R. Stephenson and S. Perkins, *Microchem. J.*, 1997, **56**, 79–92.

130 R. Ansari, M. S. Tehrani and M. B. Keivani, *J. Wood Chem. Technol.*, 2013, **33**, 19–32.

131 R. Ansari and A. F. Delavar, *J. Appl. Polym. Sci.*, 2009, **113**, 2293–2300.

132 D. F. Li, H. J. Wang, J. X. Fu, W. Wang, X. S. Jia and J. Y. Wang, *J. Phys. Chem. B*, 2008, **112**, 16290–16299.

133 R. B. Pernites, C. M. Santos, M. Maldonado, R. R. Ponnapati, D. F. Rodrigues and R. C. Advincula, *Chem. Mater.*, 2012, **24**, 870–880.